PCCP

PAPER

Combining 3-D plasmonic gold nanorod arrays with colloidal nanoparticles as a versatile concept for reliable, sensitive, and selective molecular detection by SERS†

Cite this: *Phys. Chem. Chem. Phys.*, 2014, **16**, 5563

Mehmet Yilmaz,[ab] Erhan Senlik,[ab] Erhan Biskin,[bc] Mustafa Selman Yavuz,[d] Ugur Tamer[e] and Gokhan Demirel*[ac]

The detection of molecules at an ultralow level by Surface-Enhanced Raman Spectroscopy (SERS) has recently attracted enormous interest for various applications especially in biological, medical, and environmental fields. Despite the significant progress, SERS systems are still facing challenges for practical applications related to their sensitivity, reliability, and selectivity. To overcome these limitations, in this study, we have proposed a simple yet facile concept by combining 3-D anisotropic gold nanorod arrays with colloidal gold nanoparticles having different shapes for highly reliable, selective, and sensitive detection of some hazardous chemical and biological warfare agents in trace amounts through SERS. The gold nanorod arrays were created on the BK7 glass slides or silicon wafer surfaces *via* the oblique angle deposition (OAD) technique without using any template material or lithography technique and their surface densities were adjusted by manipulating the deposition angle (α). It is found that gold nanorod arrays fabricated at $\alpha = 10^{\circ}$ exhibited the highest SERS enhancement in the absence of colloidal gold nanoparticles. Synergetic enhancement was obviously observed in SERS signals when combining gold nanorod arrays with colloidal gold nanoparticles having different shapes (*i.e.*, spherical, rod, and cage). Due to their ability to produce localized surface plasmons (LSPs) in transverse and longitudinal directions, utilization of colloidal gold nanorods as a synergetic agent led to an increase in the enhancement factor by about tenfold compared to plain gold nanorod arrays. Moreover, we have tested our approach to detect some chemical and biological toxins namely dipicolinic acid (DIP), methyl parathion (MP), and diethyl phosphoramidate (DP). For all toxins, Raman spectra with high signal-to-noise ratios and reproducibility were successfully obtained over a broad concentration range (5 ppm–10 ppb). Our results suggest that the slightly tangled and closely-packed anisotropic gold nanorod arrays reinforced by the gold nanoparticles may serve as an ideal SERS substrate to detect any analyte in trace amounts.

Received 3rd December 2013,
Accepted 23rd January 2014

DOI: 10.1039/c3cp55087g

www.rsc.org/pccp

Introduction

Surface-Enhanced Raman Spectroscopy (SERS) is a non-destructive and powerful technique that can provide ultra-sensitive and selective molecular detection of microbial pathogens, narcotics, explosives, and toxins.[1–6] Typically, Raman enhancement stems from the excitation of localized surface plasmon resonances (LSPRs), which are the collective oscillations of conduction electrons of metallic nanostructures with the incident electromagnetic field.[2] In this context, various innovative methods have been demonstrated recently either using colloidal nanoparticles or 2-D/3-D plasmonic nanostructures. Although utilization of colloidal nanoparticles for SERS applications seems to be a simple and inexpensive procedure, their uncontrolled aggregation leads to a discrepancy in the resulting SERS signals.[7,8] In contrast, reproducible and reliable SERS signals can be achieved by spatial

[a] *Bio-inspired Materials Research Laboratory (BIMREL), Department of Chemistry, Gazi University, 06500 Ankara, Turkey. E-mail: nanobiotechnology@gmail.com*
[b] *Department of Chemical Engineering, Bioengineering Division, Hacettepe University, 06800 Ankara, Turkey*
[c] *Biyomedtek: Center for Bioengineering, 06800 Ankara, Turkey*
[d] *Department of Metallurgy and Materials Engineering, Selcuk University, 42075 Konya, Turkey*
[e] *Department of Analytical Chemistry, Faculty of Pharmacy, Gazi University, 06330 Ankara, Turkey*

† Electronic supplementary information (ESI) available: TEM images and UV/Vis spectra of as-prepared colloidal nanoparticles are illustrated in Fig. S1. The SEM images of colloidal gold nanoparticles on a gold nanorod array are shown in Fig. S2. The Raman shifts, relative intensities and peak assignments for MB, DIP, DP, and MIP are shown in Tables S1–S4. See DOI: 10.1039/c3cp55087g

arrangement of metallic nanostructures, simultaneously lowering the limits of detection. These kinds of arrangements may also provide further signal enhancement in SERS due to multiple hot spot generations, cavity resonances, and propagation of SPRs.[9,10] To achieve these goals, however, sophisticated nanofabrication techniques are mostly needed and they can be costly, time-consuming and non-scalable such as electron beam lithography.[11] An alternative to creating such spatially uniform 3-D metallic nanostructures is to employ the Oblique Angle Deposition (OAD) approach which is a simple, inexpensive, maskless, and scalable vapor phase technique. By this way, various 3-D morphologies including tilted columns can be created easily on the surfaces using different metallic precursors having plasmonic features such as silver and gold.[12–14] Furthermore, intense hot spot localization, which is one of the main enhancement factors (EFs) in Raman, induced by the inter-nanostructure spacing may also be controlled in OAD through the manipulation of deposition parameters. Although spatially arranged plasmonic nanostructures provide reproducible SERS enhancement, limit of detection, infield usage, and data reliability are still challenging for practical applications.

Herein, we demonstrated a simple and versatile concept for practical SERS applications by combining 3-D anisotropic gold nanorod arrays with colloidal gold nanoparticles having varying shapes. The gold nanorod arrays having different surface densities were fabricated on the surfaces *via* the OAD technique without using any template material or lithographic technique. Three morphologies of colloidal gold nanoparticles including sphere, rod, and cage were combined with anisotropic gold nanorod arrays to evaluate synergetic SERS enhancement investigations in our work. Additionally, we demonstrated a proof of concept that indeed such synergetic enhancement in SERS signals may be utilized effectively for the detection of some important biological and chemical toxins in trace amounts.

Experimental section

Fabrication of gold nanorod arrays

The BK7 glass slides or silicon wafers were first cut (2.5 × 2.5 cm) and washed with deionized water, acetone, and piranha solution consecutively. To eliminate any contaminants, pre-cleaned surfaces were then treated with oxygen plasma at low pressure (0.2 mbar) for 30 min before gold deposition. The directional gold nanorod arrays were fabricated in a physical vapor deposition (PVD) system (NANOVAK HV, Ankara, Turkey) using a homemade OAD equipment. The thickness of deposited films was monitored using an Inficon XTM/2 deposition monitor with 0.5% sensitivity. Base pressure was gained by using a mechanical pump (Edwards E2M2 model, up to 10^{-3} Torr) and a turbo pump (Turbovac 50, up to 10^{-6} Torr) and monitored *via* a Terranova Model 934 Wide Range Vacuum Gauge Controller. During deposition, the base pressure was almost fixed at $8 \pm 1 \times 10^{-6}$ Torr with a gold evaporation rate of 0.1 Å s^{-1}. The directional gold nanorods were created at different deposition angles (*i.e.*, $\alpha = 5^{\circ}$, 10°, and 20°) to manipulate their surface densities. For comparison, smooth gold films having 32 nm of Au thickness were also fabricated at $\alpha = 90^{\circ}$.

Synthesis of gold nanoparticles (AuNPs)

The gold nanoparticles were synthesized *via* the well-known citrate reduction method[15] as follows: 50 mL of 1 mM aqueous solution of $HAuCl_4$ was transferred to a three-neck round bottom flask. The mixture was heated to boiling while stirring vigorously. Afterwards, trisodium citrate solution (0.1 M, 1.65 mL) was added to the boiling mixture. After cooling to room temperature, the samples were then centrifuged and washed with DI water several times and re-dispersed in water.

Synthesis of gold nanorods (AuNRs)

The AuNRs were synthesized by a two-step seeding method described by Nikoobakht and El-Sayed.[16] In the first step, freshly-prepared ice cold sodium borohydride (0.02 M, 0.15 mL) was added to the mixture of $HAuCl_4$ (1 mM, 2.5 mL) and cetyltrimethylammonium bromide (CTAB) (0.5 M, 2 mL) all at once. The solution was vigorously stirred at room temperature for 5 min. The brownish color indicates the formation of seed solution. The seed solution was used for the synthesis of gold nanorods within 30 min. 18 μL of the freshly prepared seed solution was added to growth solution containing $HAuCl_4$ (2.5 mL, 1 mM), CTAB (2 mL, 0.5 M), silver nitrate (0.5 mL, 1 mM) and L-ascorbic acid (0.25 mL, 0.1 M) under magnetic stirring. The synthesis was prolonged for 20 minutes for completion. The pinkish-red colored solution was centrifuged and washed three times with DI water to remove excess amounts of CTAB.

Synthesis of gold nanocages (AuNCs)

The AuNCs were prepared *via* the galvanic replacement reaction between silver (Ag) nanocubes and chloroauric acid ($HAuCl_4$). In the first step, Ag nanocubes were synthesized by a previously described protocol.[17] Afterward, as-prepared Ag nanocubes in a fixed amount ($\sim$3 nM) were dispersed in aqueous solution of poly(vinylpyrrolidone) (PVP) in a flask under magnetic stirring. This mixture was heated to boiling for 10 min. A $HAuCl_4$ solution (3 mL, 0.2 mM) was then added into the flask through a syringe pump under magnetic stirring. The heating of this solution for another 10 min resulted in a stable color of the system. The cooled sample was centrifuged and saturated NaCl solution was employed to remove AgCl. Finally, the solution was washed with water several times to discard PVP and NaCl before further use.

SERS measurements

For all Raman studies, a Delta Nu Examiner Raman Microscopy system equipped with a 785 nm laser source, a motorized microscope stage sample holder, and a cooled charge-coupled device (CCD) detector was used in the range of 200–2000 cm^{-1}. Instrument parameters were as follows: 20X objective, 30 μm spot size, 30 s acquisition time, 150 mW laser power and baseline correction was performed for all measurements. Before the SERS measurement, UV-ozone cleaning was applied to gold nanorod arrays and smooth gold films to remove any contamination on the surfaces for 10 min. To evaluate the SERS enhancement, a methylene blue (MB) solution (10 μM) was

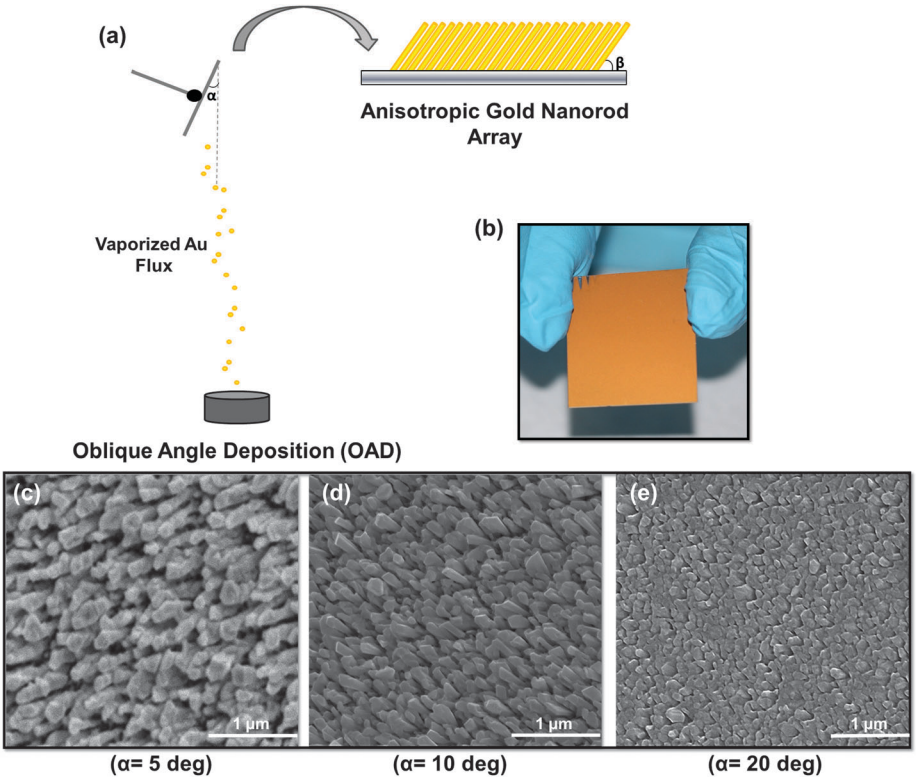

Fig. 1 Schematic representation of the OAD process (a), optical image of a surface after deposition of gold (b), and top-view SEM images of fabricated gold nanorod arrays (GNA) at 5° (c), 10° (d), and 20° of deposition angles (e).

prepared with or without colloidal gold nanoparticles having different shapes. The gold nanoparticle concentrations in the mixture were altered in the range of 0–20 ppm. Afterwards, 3 μL of an aqueous solution of MB with or without gold nanoparticles is dropped onto the smooth and anisotropic gold nanorod arrays and kept in a hood until dry. In the case of toxin samples, an almost similar procedure was applied except the employment of toxins at desired concentration instead of MB. The drying procedure created coin-shaped Raman sample sizes of 4 ± 1 mm onto the gold substrates. For each sample, at least ten Raman spectra were collected from the different spots of substrate to determine the reproducibility and homogeneity.

To demonstrate the electric field distribution and generation of hot spots on the related substrates, finite element modeling was applied to gain the numerical solution of partial differential equations for variable geometries by using the commercial COMSOL software package. The simulations were restricted to 2-D models of gold nanorod arrays ($\beta = 65^\circ$ for $\alpha = 10^\circ$) with 100 nm nanorod radius and 10 nm inter-nanorod distance with or without AuNRs, so that fast and reliable modeling can be assured. In this model, all necessary physical principles and material properties are included.

Results and discussion

In the first step, we fabricated anisotropic gold nanorod arrays having varying surface densities onto the silicon or glass surfaces *via* the OAD technique. Demirel and co-workers recently showed that directional gold nanorod arrays with different tilt angles (β) can easily be fabricated on solid surfaces through the OAD approach and their surface densities can be manipulated by controlling their deposition angles.[14] Fig. 1 shows the schematic representation of the fabrication process of anisotropic gold nanorod arrays and their top-view SEM images, which were deposited at different deposition angles (*i.e.*, $\alpha = 5^\circ$, 10°, and 20°). Obviously, the final morphology of the nanostructured gold surfaces changed with the deposition angle. In the case of 5° and 10° of deposition angles, closely packed and tilted gold nanorod arrays were easily detected (Fig. 1c and d). The nanorod densities were calculated *via* freeware IMAGEJ software and found to be 3.86×10^8 nanorods cm^{-2} for $\alpha = 5^\circ$ and 5.63×10^8 nanorods cm^{-2} for $\alpha = 10^\circ$, respectively. Interestingly, increasing the deposition angle from 10° to 20° caused a dramatic change in the morphology of deposited gold onto the surfaces. A rough gold film instead of nanorod like morphologies was observed for 20° of deposition angle possibly due to the lack of the self-shadowing effect of vaporized gold during growth (see Fig. 1e). Parallel to our results, Kubus *et al.* previously demonstrated that increasing the deposition angle led to a remarkable decrease in surface roughness as well as disappearance of gold nanorod arrays.[14]

The slightly tangled and ordered 3-D nanoarrays of noble metals compared with 1-D and 2-D structures offer unique advantages including increased surface area, promoting the formation of hot spots and the capture of target molecules.[9]

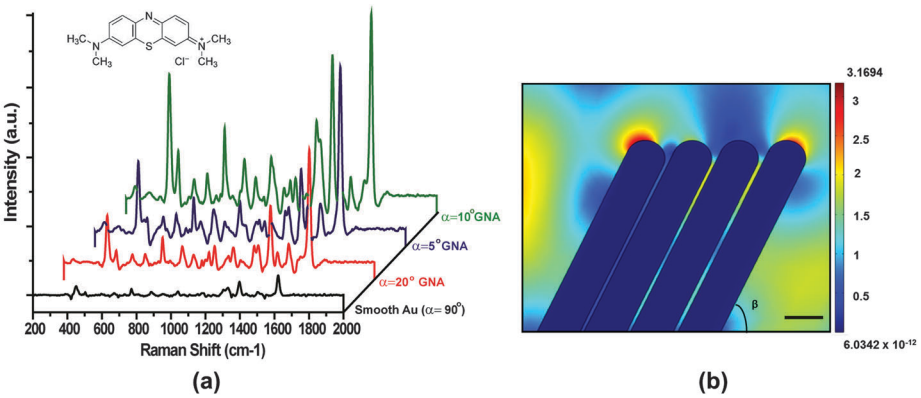

Fig. 2 (a) SERS spectra of MB (10 μM) on gold nanorod arrays (GNA) deposited at different deposition angles (α) (inset shows the chemical structure of MB) and (b) electric field distribution of an anisotropic gold nanorod array (β = 65° for α = 10°) for excitation of localized surface plasmon resonance (scale bar is 100 nm).

In this context, we envisioned that our anisotropic gold nanorod arrays with varying surface densities would be a promising SERS substrate for practical applications. To evaluate the SERS performances of deposited gold nanorod arrays, we used methylene blue (MB) as a reporter molecule. Typically, a certain amount of aqueous solution of MB (3 μL, 10 μM) was first dropped onto the fabricated surfaces and kept at room temperature until drying. Fig. 2a shows the SERS spectra of MB on anisotropic gold nanorod arrays deposited at different deposition angles. A smooth gold surface with α = 90° was also utilized for comparison. We observed that all collected spectra are precise and have high signal-to-noise ratios consistent with most of the reports for MB (Table S1, ESI†).[18–20] For all cases, the most prominent peaks in the spectra of MB are the ring stretch (ν(C–C)) at ~1610 cm^{-1}, symmetric and asymmetric C–N stretches (ν_{sym}(C–N) and ν_{asym}(C–N)) at ~1396 and ~1436 cm^{-1}, respectively, and the C–N–C skeletal deformation mode (δ(C–N–C)) at 449 cm^{-1}. The signal-to-noise ratios (S/N) for the substrates fabricated at 5°, 10°, and 20° of deposition angles were also calculated as the ratio of intensity of the signal at ~1610 cm^{-1} over the background noise. The S/N ratios were determined to be 46 ± 4 for α = 10°, 36 ± 6 for α = 5°, and 24 ± 8 for α = 10°, respectively. The employment of deposited gold films, especially at α = 5° and 10°, resulted in higher SERS enhancement compared with the smooth gold surface. Although we mentioned earlier that there was no obvious nanorod structure for 20° of deposition angle, a dramatic increment in the SERS signal relative to the smooth gold surface was also detected possibly due to surface roughness and tangled structure of deposited film. In the cases of 5° and 10° of deposition angles, we perceive that the resulting SERS enhancement may be possibly due to the intense hot spot formations and easy access of target molecules to the hot spots.[9] When considering the hot spot formations, the tips of gold nanorods are mainly responsible for the generation of hot spots having an extremely high electric field enhancement due to the tip-focusing, cavity resonances and nano-antenna effects besides the longitudinal and transverse localized surface plasmon resonance (LSPR) modes of the nanorod itself (Fig. 2b).[9,10,20] For instance, cavity resonance, which is a typical near-field character and has a strong effect on SERS signal enhancement, is created by nanorods arranged side by side at quite short distances.[10] Inter-nanorod distances in GNA were calculated from SEM images using the IMAGEJ software and found to be ~50–200 nm for α = 5° and ~10–100 nm for α = 10°. Moreover, resultant nanorod arrays also provide a larger dynamic sensing area, average enhancement over the sample surface instead of point enhancement, and significant reduction in signal fluctuation.[21] Additionally, thanks to ordered nanorod arrays, SPRs propagate among nanorod arrays causing the formation of propagating SPRs. Consistent with our explanations, one of the authors in our work recently showed that anisotropic gold nanorod arrays have a strong surface plasmon resonance, which indicates dense polariton formation and propagating SPRs.[22] All of these mentioned contributions play an important role to some degree in observed SERS signal enhancements. As for comparing the runs for 5° and 10° of deposition angles, anisotropic gold nanorod array deposited at 10° exhibited higher SERS intensity than the surfaces fabricated at 5° because of higher nanorod density.

In order to compare SERS enhancements of fabricated surfaces, we also calculated the SERS enhancement factors (EF) by applying the following equation using the Raman intensity peak of MB at ~1610 cm^{-1}:

$$EF = (N_{bulk} \times I_{gold\ film})/(N_{gold\ film} \times I_{bulk})$$

where I_{bulk} and $I_{gold\ film}$ are the Raman intensities of pure bulk MB and the adsorbed MB on the gold nanorod films and the N_{bulk} and $N_{gold\ film}$ are the number of MB molecules for the reference sample (in our case the smooth gold surface deposited at α = 90°) and gold nanorod arrays deposited at different deposition angles. The calculated EFs are 7.2 × 10^5 for α = 10°, 2.2 × 10^5 for α = 5° and 3.4 × 10^4 for α = 20°, respectively. It should be noted that these EFs are average SERS EFs which indicate the SERS signal averaged over the entire area of interrogation not isolated hot spots.

In addition to these explanations, we should note that our fabricated substrates have tilted gold nanorods; therefore, their

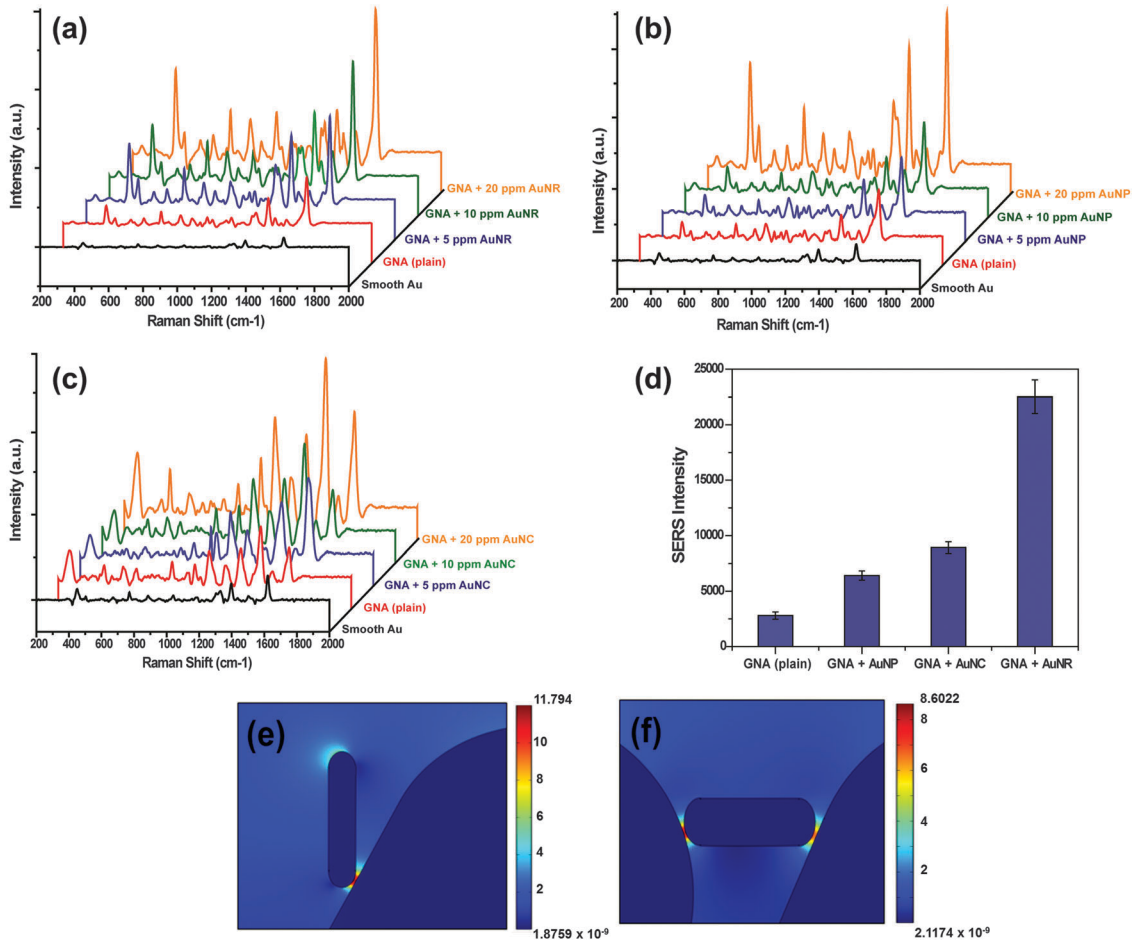

Fig. 3 (a) SERS spectra of MB on gold nanorod arrays (GNA) fabricated at 10° of deposition angle in the presence of colloidal gold nanorods (AuNR), (b) spherical gold nanoparticles (AuNP), and (c) gold nanocages (AuNC) (insets show the TEM images of AuNR, AuNP, and AuNC). (d) SERS enhancement comparison for colloidal gold nanoparticles having different shapes, and (e and f) electric field distribution of a single gold nanorod on an anisotropic gold nanorod array (β = 65° for α = 10°) for excitation of localized surface plasmon resonance for different orientations of AuNRs.

SERS responses were affected by the angle of incident laser. In the literature, several studies have been done to investigate angular dependence of SERS using anisotropic nanorod arrays.[23–26] Zhao and co-workers have reported that the SERS intensities of tilted silver nanorod arrays changed with the incident angle of laser and the maximum SERS intensity was observed at about 45° which is about five times the intensity at 90°.[23] In another work, Zhao *et al.* have also found that anisotropic silver nanorod arrays showed an anisotropy of the SERS polarization different from the polarized UV-vis absorbance.[26] In the same work, the maximum SERS intensity was observed in the polarization direction perpendicular to the long axis of the silver nanorods, while the UV-vis absorbance was strongly polarized along the direction of the long axis of the nanorod array. However, they could not observe any obvious change in the SERS intensities depending on the incoming polarization angle. One of the authors in our work recently reported that tilted gold nanorod arrays showed a strong plasmon resonance, when the incoming light comes through the gold nanorods along the anisotropic axis.[22] If the incoming light is aligned with the isotropic axis, these resonance bands were shifted to a higher energy value and became broadened. The observed variation in the plasmonic behavior may have been caused by the polarization of light. The p-polarization has the electric field vector oscillating normal to the plane of the nanorods along the anisotropic axis. Thus, it can excite surface plasmons. In this case, the excitation by s-polarization can be neglected. However, the electric field vector of p-polarization is oriented parallel to the nanorods along the isotropic axis and as a result it cannot excite plasmons sufficiently, and the surface plasmons are mainly excited by s-polarization. In light of our preliminary studies and related literature, we believe that illumination of laser at 90° to anisotropic gold nanorod arrays may sufficiently excite SPR and induce SERS enhancement possibly due to the SPR excitations by both p- and s-polarizations. However, in order to get maximum SPR excitation for biosensor applications, we are still working on this issue.

The SERS studies performed with MB was notably promising but not in required proportion for the detection of any analyte in trace amounts. For this reason, we proposed a novel concept to obtain higher, reliable, and reproducible SERS enhancement. The use of colloidal gold nanoparticles having varying

shapes and sizes as an SERS platform is a well-known strategy and can be adapted to nearly all systems because of their tunable optical properties, long-term stabilities, and high compatibilities with most of the analytes.[27–29] Therefore, we envisioned that combining anisotropic gold nanorod arrays with colloidal gold nanoparticles having different shapes may exhibit some remarkable progress in SERS studies. Within the scope of this study, colloidal gold nanoparticles in three different shapes, spherical (AuNPs), rod (AuNRs) and cage (AuNCs), were synthesized according to methods described in the Experimental section. Obviously, all nanoparticles were successively obtained in quite narrow size distributions (Fig. S1d–f, ESI†). The SPR properties of nanoparticles were also in good agreement with TEM data (Fig. S1a–c, ESI†).

After these experiments, to evaluate the synergetic enhancement, MB solutions were first mixed with colloidal gold nanoparticles having different shapes (*i.e.*, AuNPs, AuNRs and AuNCs). In the resultant mixture, nanoparticle concentrations were changed in the range of 5 ppm to 20 ppm. Afterwards, these mixtures were dropped onto the gold nanorod arrays deposited at $\alpha = 10^{\circ}$. Fig. 3a–c represents the data acquired from different colloidal gold nanoparticles at varying concentrations on gold nanorod arrays. For comparison, SERS spectra of MB for smooth and gold nanorod arrays without using any colloidal nanoparticles are given in the same figure. The employment of colloidal nanoparticles even at low concentration (5 ppm) caused an increment in the SERS intensity without any change in band characteristics. In the presence of 20 ppm colloidal gold nanoparticles, the EFs were calculated to be 4.7×10^6 for GNA + AuNRs, 8.2×10^5 for GNA + AuNCs, and 9.1×10^4 for GNA + AuNPs, respectively. The enhancement in SERS signals in the presence of colloidal gold nanoparticles may be attributed to the electromagnetic coupling effect of colloidal gold nanoparticles on/in two or more gold nanorod arrays with small distance. The junctions of nanoparticles in different architectures with gold nanorod arrays make enormous contribution to the formation of hot spots and resulted in an additional SERS improvement (see Fig. 3d and Fig. S2, ESI†). In the presence of AuNPs, the Raman signal was increased effectively but not in a desired proportion. On the other hand, the enhancement for AuNCs and especially in the presence of AuNRs is quite satisfying. These results may be attributed to SPR properties, shapes and architectures of the utilized nanoparticles. The AuNPs with a smooth surface can be limited to create sufficient hot spots on nanorod arrays. At the same time, due to the small particle size of synthesized spherical gold nanoparticles, our incident laser source may not excite effectively the surface plasmons of gold nanoparticles. In parallel to this reason, additional SERS enhancement by the spherical gold nanoparticles could not be obtained. In the case of AuNCs, equidistant sharp edges facilitated the formation of a larger number of localized plasmons.[30] As for the use of AuNRs on gold nanorod arrays also led to desired improvement in the SERS signal (Fig. 3e and f). We perceive that the remarkable increment in the Raman signal in the presence of AuNRs may be attributed to their ability to produce localized plasmons in transverse and longitudinal directions.[11,31,32] The colloidal AuNRs, which were used for the decoration of gold nanorod arrays, have two distinct SPR absorption peaks. The strong SPR peak positioned at 746 nm is due to the resonant propagation of surface plasmons along the longitudinal axis and the weaker SPR peak centered at around 528 nm also stems from the propagating surface plasmons along the transverse axis. In our work, we have employed an excitation laser source having a

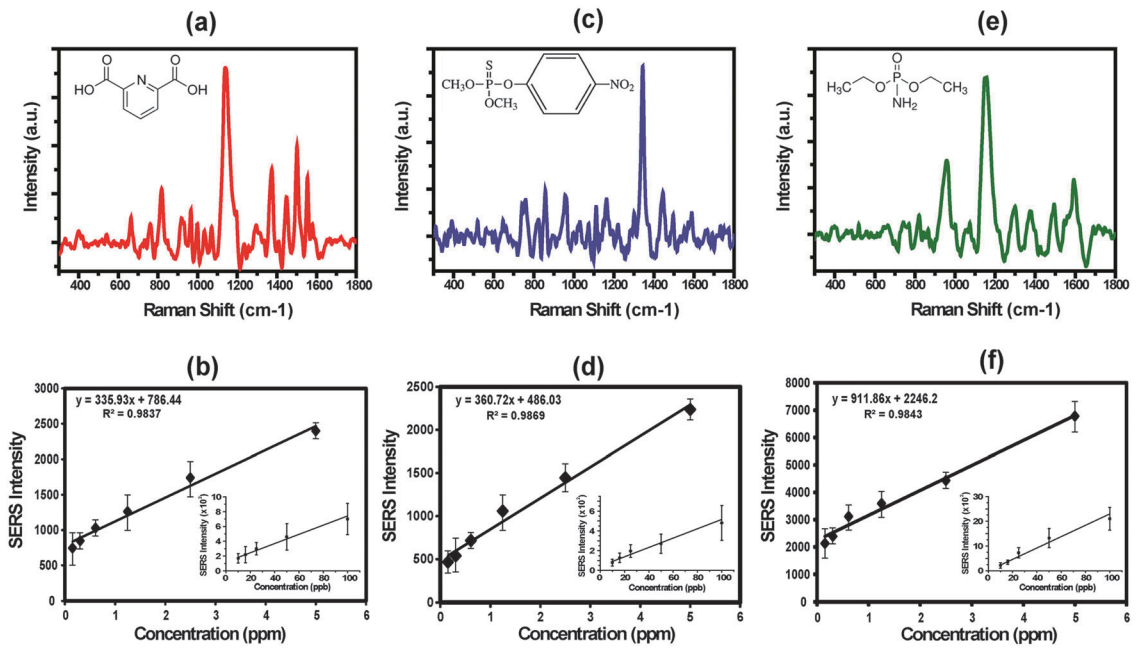

Fig. 4 SERS spectra and related calibration curves for DIP (a and b), MP (c and d), and DP (e and f). Insets show the chemical structures of DIP, MP and DP.

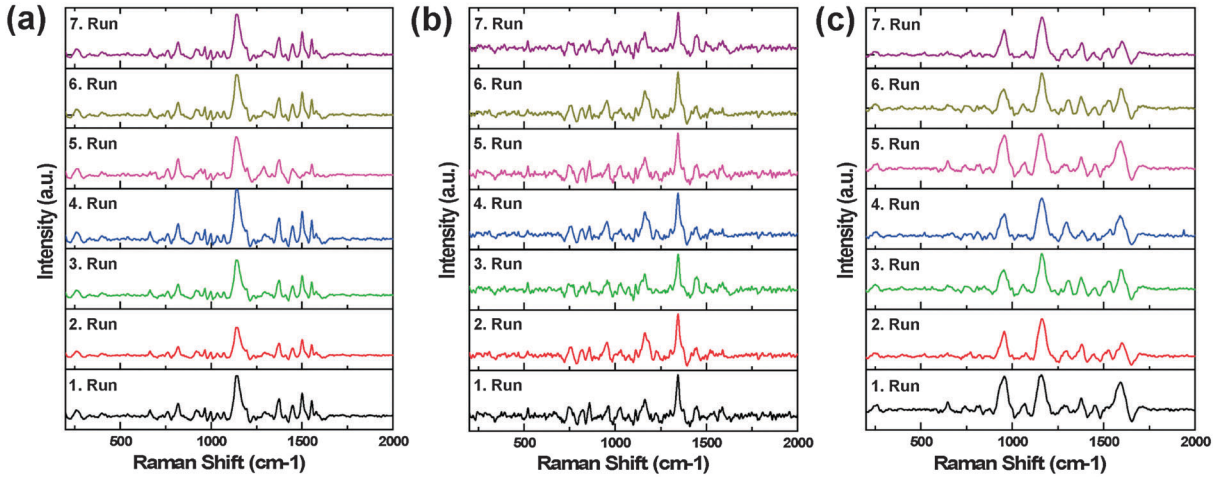

Fig. 5 Reproducible SERS spectra for 5 ppm of DIP (a), MP (b), and DP (c) on gold nanorod arrays in the presence of 20 ppm colloidal AuNRs.

wavelength of 785 nm, which is quite close to the SPR peak of colloidal AuNRs centered at 746 nm. This provides the maximization of the magnitude of the local electric field at the interface between the surface of the colloidal AuNR and the gold nanorod array responsible for the observed SERS enhancement.

As a proof-of-concept, by using our approach, we investigated the detection of some important chemical and biological warfare agents namely dipicolinic acid (DIP), methyl parathion (MP) and diethyl phosphoramidate (DP). In a typical experiment, an appropriate amount of each toxin solution (5 ppm–10 ppb) was first mixed with AuNR solution (20 ppm) for 1 h. Afterwards, 3 μL of these mixtures were dropped onto gold nanorod arrays fabricated at 10° of deposition angle and kept under room conditions in a hood to dry. Fig. 4 illustrates the representative Raman spectra of selected toxin agents. For all toxins, we observed strong Raman signals for all concentration ranges with high signal-to-noise ratios (Fig. 4a, c, and e). The characteristic bands of each toxin were compared with related literature and high compatibility was observed (Tables S2–S4, ESI†).[33] The most prominent peak of DIP, MP and DP at bands of 1150, 1340 and 1170 cm^{-1}, respectively, was selected to determine the dependency of Raman intensities on toxin concentration. The intensities of related bands increased with the concentration of toxin molecules (Fig. 4b, d, and f). The detection limit for all toxin molecules was found to be almost the same and about 10 ppb. A relatively good linearity was also detected over a wide range of concentrations with acceptable R^2 (coefficient of determination) for reliable calibration studies.

Finally, we evaluated the reproducibility of SERS spectra, which were obtained from our systems, using aforementioned toxin molecules. To demonstrate the reproducibility of our proposed system, numerous signals were collected from the different spots of the SERS substrate for the case study of 5 ppm of all toxins and 20 ppm of AuNRs as final concentrations on gold nanorod arrays. We could obtain SERS spectra for all toxins with high reproducibility. From spot to spot, the most prominent peak of DIP, MP and DP at bands of ~1150, ~1340 and ~1170 cm^{-1} shows a relative intensity deviation of ~18% (Fig. 5). The quite high reproducibility data are strong proof of the uniform distribution of the hot spots over the Raman spot size and make our proposed system, consisting of gold nanorod arrays and colloidal gold nanorods, a potent candidate for universal SERS substrates.

Conclusions

In summary, we report a simple yet very effective approach by combining gold nanorod arrays and colloidal gold nanoparticles for practical SERS applications. In the absence of colloidal gold nanoparticles, anisotropic gold nanorod arrays fabricated at 10° of deposition angle exhibited the highest SERS enhancement. A remarkable synergetic enhancement in SERS signals was obviously observed, when combining gold nanorod arrays with colloidal gold nanoparticles having different shapes (*i.e.*, spherical, rod, and cage). It is found that among the colloidal gold nanoparticles, nanorods (AuNRs) led to a more intense Raman signal. Additionally, we have employed our concept to detect some chemical and biological toxins. For all toxins, Raman spectra over a broad concentration range (5 ppm–10 ppb) were successfully collected with high signal-to-noise ratios and reproducibility. Although there are still many challenges ahead related to SERS, the present concept can be regarded as an important step towards the fabrication of a universal SERS platform and may open up intriguing opportunities for practical SERS applications.

Acknowledgements

This work was supported by the Scientific and Technological Research Council (TUBITAK) grant numbers 111M237 and 112T560. MY is supported by TUBITAK BIDEB fellowship. EP also acknowledges support from the Turkish Academy of Science as a full member. The authors would like to thank Hakan Erdogan for useful discussions.

References

1 M. Moskovits, *J. Raman Spectrosc.*, 2005, **36**, 485–496.
2 P. L. Stiles, J. A. Dieringer, N. C. Shah and R. R. Van Duyne, *Annu. Rev. Anal. Chem.*, 2008, **1**, 601–626.
3 R. M. Jarvis and R. Goodacre, *Chem. Soc. Rev.*, 2008, **37**, 931–936.
4 A. G. Ryder, *Curr. Opin. Chem. Biol.*, 2005, **9**, 489–493.
5 A. Chou, E. Jaatinen, R. Buividas, G. Seniutinas, S. Juodkazis, E. L. Izake and P. M. Fredericks, *Nanoscale*, 2012, **4**, 7419–7424.
6 Y. Zhu, H. Kuang, L. Xu, W. Ma, C. Peng, Y. Hua, L. Wang and C. Xu, *J. Mater. Chem.*, 2012, **22**, 2387–2391.
7 J. F. Li, Y. F. Huang, Y. Ding, Z. L. Yang, S. B. Li, X. S. Zhou, F. R. Fan, W. Zhang, Z. Y. Zhou and D. Y. Wu, *Nature*, 2010, **464**, 392–395.
8 M. P. Cecchini, V. A. Turek, J. Paget, A. A. Kornyshev and J. B. Edel, *Nat. Mater.*, 2012, **12**, 165–171.
9 W. Wei, K. Chen and G. Ge, *Adv. Mater.*, 2013, **25**, 3863–3868.
10 M. D. Doherty, A. Murphy, J. McPhillips, R. J. Pollard and P. Dawson, *J. Phys. Chem. C*, 2010, **114**, 19913–19919.
11 R. A. Tripp, R. A. Dluhy and Y. Zhao, *Nano Today*, 2008, **3**, 31–37.
12 X. Wang, J. Abell, Y. P. Zhao and Z. Zhang, *Appl. Opt.*, 2012, **51**, 1521–1531.
13 Q. Zhou, X. Zhang, Y. Huang, Z. Li, Y. Zhao and Z. Zhang, *Appl. Phys. Lett.*, 2012, **100**, 113101.
14 L. Kubus, H. Erdogan, E. Piskin and G. Demirel, *Soft Matter*, 2012, **8**, 11704–11707.
15 H. Erdogan, H. Sakalak, M. S. Yavuz and G. Demirel, *Langmuir*, 2013, **29**, 6975–6982.
16 B. Nikoobakht and M. A. El-Sayed, *Chem. Mater.*, 2003, **15**, 1957–1962.
17 M. S. Yavuz, Y. Cheng, J. Chen, C. M. Cobley, Q. Zhang, M. Rycenga, J. Xie, C. Kim, K. H. Song and A. G. Schwartz, *Nat. Mater.*, 2009, **8**, 935–939.
18 L. Li, T. Hutter, A. S. Finnemore, F. M. Huang, J. J. Baumberg, S. R. Elliott, U. Steiner and S. Mahajan, *Nano Lett.*, 2012, **12**, 4242–4246.
19 Q. Hao, B. Wang, J. A. Bossard, B. Kiraly, Y. Zeng, I.-K. Chiang, L. Jensen, D. H. Werner and T. J. Huang, *J. Phys. Chem. C*, 2012, **116**, 7249–7254.
20 P. Ghenuche, S. Cherukulappurath, T. H. Taminiau, N. F. van Hulst and R. Quidant, *Phys. Rev. Lett.*, 2008, **101**, 116805.
21 A. Kabashin, P. Evans, S. Pastkovsky, W. Hendren, G. Wurtz, R. Atkinson, R. Pollard, V. Podolskiy and A. Zayats, *Nat. Mater.*, 2009, **8**, 867–871.
22 L. Kubus, H. Erdogan, S. S. Cetin, E. Biskin and G. Demirel, *ChemCatChem*, 2013, **5**, 2973–2977.
23 Y. Liu, J. Fan and Y. P. Zhao, *Appl. Phys. Lett.*, 2006, **89**, 173134.
24 Y. J. Liu, H. Y. Chu and Y. P. Zhao, *J. Phys. Chem. C*, 2010, **114**, 8176–8183.
25 Y. J. Liu and Y. P. Zhao, *Phys. Rev. B: Condens. Matter Mater. Phys.*, 2008, **78**, 075436.
26 Y. P. Zhao, S. B. Chaney and R. A. Dluhy, *J. Phys. Chem. B*, 2006, **110**, 3153–3157.
27 M. E. Pekdemir, D. Ertürkan, H. Külah, İ. H. Boyacı, C. Özgen and U. Tamer, *Analyst*, 2012, **137**, 4834–4840.
28 M. K. Khaing Oo, Y. Guo, K. Reddy, J. Liu and X. Fan, *Anal. Chem.*, 2012, **84**, 3376–3381.
29 P. Pinkhasova, L. Yang, Y. Zhang, S. Sukhishvili and H. Du, *Langmuir*, 2012, **28**, 2529–2535.
30 G. P. Kumar, *J. Nanophotonics*, 2012, **6**, 064503.
31 S. Lal, N. K. Grady, J. Kundu, C. S. Levin, J. B. Lassiter and N. J. Halas, *Chem. Soc. Rev.*, 2008, **37**, 898–911.
32 J. Kumar and K. G. Thomas, *J. Phys. Chem. Lett.*, 2011, **2**, 610–615.
33 F. Yan and T. Vo-Dinh, *Sens. Actuators, B*, 2007, **121**, 61–66.

